JOURNAL OF GEOPHYSICAL RESEARCH, VOL. 114, D13304, doi:10.1029/2008JD010560, 2009

Observed vertical distribution of tropospheric ozone during the Asian summertime monsoon

John Worden,[1] Dylan B. A. Jones,[2] Jane Liu,[2] Mark Parrington,[2] Kevin Bowman,[1] Ivanka Stajner,[3] Reinhard Beer,[1] Jonathan Jiang,[1] Valérie Thouret,[4] Susan Kulawik,[1] Jui-Lin F. Li,[1] Sunita Verma,[1] and Helen Worden[5]

Received 6 June 2008; revised 27 March 2009; accepted 27 April 2009; published 10 July 2009.

[1] We characterize the horizontal and vertical distribution of tropospheric ozone measured by the Tropospheric Emission Spectrometer (TES) over North Africa, the Middle East, and Asia. Studies have shown that the summertime circulation associated with the Asian monsoon significantly influences the spatial distribution of ozone and its precursors. However, there have been limited observations of the distribution of tropospheric ozone over this region. Over the Middle East, TES observations reveal abundances of ozone between 60 and 100 ppbv, with amounts over 80 ppbv typically occurring between 300 and 450 hPa, whereas over India, enhanced ozone abundances are near 300 hPa. Over central Asia, observed ozone amounts are 150–200 ppbv at altitudes near 300 hPa. These enhanced ozone abundances are observed in June and July, corresponding to the onset of the Asian monsoon, and begin to dissipate in August. Intercomparison of the TES data with ozone climatologies derived from the Measurements of Ozone and Water Vapor by in-Service Airbus Aircraft program show that the TES ozone is biased high by about 15% between 300 and 750 hPa, consistent with prior validation studies. Comparison of the assimilation of TES data into the GEOS-Chem model with assimilation of data from the Microwave Limb Sounder (MLS) and the Ozone Monitoring Instrument (OMI) into the Goddard Earth Observing System (GEOS-4) model shows consistency in the distribution of ozone. For example, at 7–8 km across North Africa, the Middle East, and Asia the bias between GEOS-Chem and the assimilated OMI and MLS fields was reduced from 6.8 to 1.4 ppbv following assimilation of the TES data.

Citation: Worden, J., et al. (2009), Observed vertical distribution of tropospheric ozone during the Asian summertime monsoon, *J. Geophys. Res.*, *114*, D13304, doi:10.1029/2008JD010560.

1. Introduction

[2] The summertime Asian Monsoon profoundly affects the climate over North Africa, the Middle East and Central Asia [*Hoskins and Rodwell*, 1995; *Dunkerton*, 1995; *Rodwell and Hoskins*, 1996, 2001]. However, only recently have observations begun to provide understanding on how the Asian Monsoon affects the chemical composition of the troposphere. These observations reveal a complex system involving deep convective transport of boundary layer air to the upper troposphere [*Fu et al.*, 2006; *Gettelman et al.*, 2004], followed by entrainment into the upper tropospheric anticyclone that forms during summer in this region [*Barret et al.*, 2008; *Park et al.*, 2008, 2007; *Randel and Park*, 2006; *Kunhikrishnan et al.*, 2006]. For example, space-based observations from the Measurements of Pollution in the Troposphere (MOPITT) [*Kar et al.*, 2004] instrument, the Microwave Limb Sounder (MLS) [*Jiang et al.*, 2007; *Park et al.*, 2007], the Atmospheric Composition Experiment (ACE) [*Park et al.*, 2008], and the Atmospheric Infrared Sounder (AIRS) [*Randel and Park*, 2006] have shown how deep convective transport associated with the Asian monsoon lofts boundary layer air with low abundances of ozone and high concentrations of water and CO into the upper troposphere [*Fu et al.*, 2006; *Gettelman et al.*, 2004].

[3] On the basis of modeling simulations using the GEOS-Chem model, it was suggested by *Li et al.* [2001] that enhanced summertime ozone abundances (greater than 80 ppbv) should be observed in the middle troposphere over Africa the Middle East. This prominent feature in the GEOS-Chem model was shown by *Li et al.* [2001] to be linked to the anticyclone which forms in response to the Asian Monsoon. They argued that NOx production from lightning together with ozone precursors transported from Asia were critical for the photochemical buildup of ozone in

[1]Jet Propulsion Laboratory, California Institute of Technology, Pasadena, California, USA.
[2]Department of Physics, University of Toronto, Toronto, Ontario, Canada.
[3]Noblis, Incorporated, Falls Church, Virginia, USA.
[4]Laboratoire d'Aérologie, UMR5560, Université de Toulouse, CNRS, Toulouse, France.
[5]National Center for Atmospheric Research, Boulder, Colorado, USA.

0148-0227/09/2008JD010560$09.00

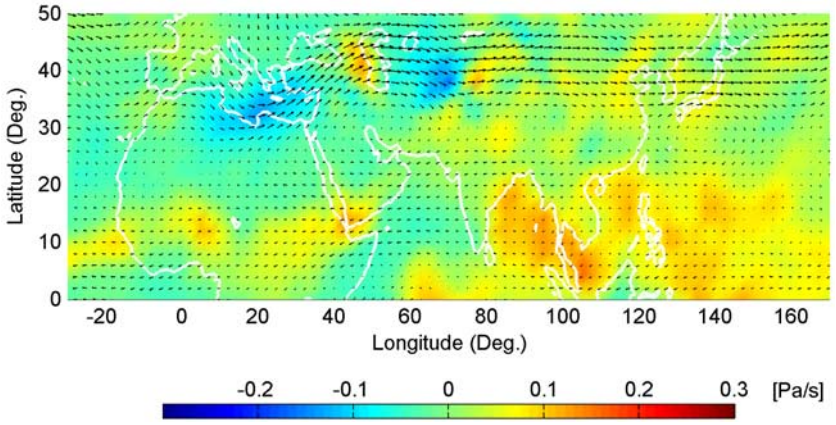

Figure 1. Monthly mean horizontal winds (arrows) and vertical velocity (in Pa/s) for July 2006 produced by the GEOS-4 data assimilation system at 8–9 km. Vertical ascent is indicated by the red colors, while descent is shown in blue.

the region. Observations using solar occultation, as discussed by *Kar et al.* [2002], do suggest the existence of peak ozone amounts at about 7 km altitude over North East Africa and North West Saudi Arabia relative to the rest of the globe. However, observations of total tropospheric ozone from the Ozone Monitoring Instrument (OMI) and the Global Ozone Monitoring Instrument (GOME) show that tropospheric ozone columns are generally enhanced between the latitudes of 25°–35°N, particularly over Northwest Saudi Arabia [*Liu et al.*, 2006], and the GOME data do not show peak ozone abundances over the eastern hemisphere relative to the western hemisphere [*Liu et al.*, 2006].

[4] Model predictions as well as satellite observations of tropospheric ozone suggest that the vertical and horizontal distribution of ozone varies strongly in response to the dynamics of the Asian Monsoon. Shown in Figure 1 are the vertical velocities and horizontal winds in the upper troposphere associated with the Asian monsoon, as reproduced by the NASA Global Modeling and Analysis Office (GMAO) assimilation system [*Bloom et al.*, 2005]. There is strong upward convective transport over the monsoon region and localized descent over North Africa and central Asia. In addition to the large-scale anticyclone in the upper troposphere over Tibet, there is a secondary anticyclone over the Persian Gulf, which is stronger in the middle troposphere. Understanding how the distribution of ozone in the middle and upper troposphere is influenced by these dynamical processes and the local in situ photochemistry has both climate and air quality implications. Upper tropospheric ozone is an important greenhouse gas that affects global outgoing longwave radiation [*Worden et al.*, 2008] and the summertime buildup of ozone in the region will enhance background ozone abundances, which can impact air quality if it is transported to the boundary layer [*Fiore et al.*, 2002].

[5] In this paper we present the Tropospheric Emission Spectrometer (TES) vertical profile observations of tropospheric ozone obtained during the summers of 2005, 2006, and 2007. We show the temporal, horizontal, and vertical distribution of tropospheric ozone across northeast Africa, the Middle East, and Asia and quantify the bias and errors in the TES data over this region. The TES data are compared with aircraft measurements of ozone by the Measurements of Ozone and Water Vapor by in-Service Airbus Aircraft (MOZAIC) program for pressures between 300 and 700 hPa over Delhi, Teheran, and Dubai [*Marenco et al.*, 1998] (http://mozaic.aero.obs-mip.fr/web/). We also assess the consistency of the information on the vertical distribution of ozone provided by the TES and MLS data when the data are assimilated into atmospheric models. Characterizing the spatial and temporal variability of ozone in this region is a critical first step toward understanding how the dynamics and chemistry controls the ozone distribution and for quantifying the sources of ozone precursors. In a companion study, *Liu et al.* [2009] conducted a detailed modeling analysis to better understand the transport and chemical processes responsible for observed ozone enhancements across North Africa and the Middle East.

2. TES Instrument

[6] The TES instrument is an infrared, high resolution, Fourier Transform spectrometer covering the spectral range between 650 to 3050 cm^{-1} (15.4 to 3.3 μm) with an apodized spectral resolution of 0.1 cm^{-1} for the nadir view [*Beer et al.*, 2001]. Spectral radiances measured by TES are used to infer atmospheric profiles using a nonlinear optimal estimation algorithm that minimizes the difference between these radiances and those calculated with the equation of radiative transfer, subject to the constraint that the parameters are consistent with a statistical a priori description of the atmosphere [*Bowman et al.*, 2006; *Rodgers*, 2000]. TES provides a global view of tropospheric trace gas profiles including ozone, water vapor, and carbon monoxide, along with atmospheric temperature, surface temperature and emissivity, effective cloud top pressure, and effective cloud optical depth [*Kulawik et al.*, 2006; *Worden et al.*, 2004]. For cloud free conditions, the vertical resolution of TES ozone profile retrievals is typically 6 km in the tropics and at midlatitudes in summers [*Jourdain et al.*, 2007; *Worden et al.*, 2004]. Tropospheric ozone retrievals from TES have been validated against ozonesonde and lidar measurements and it is generally found that the values are biased high by as much as 15% after accounting for the TES vertical

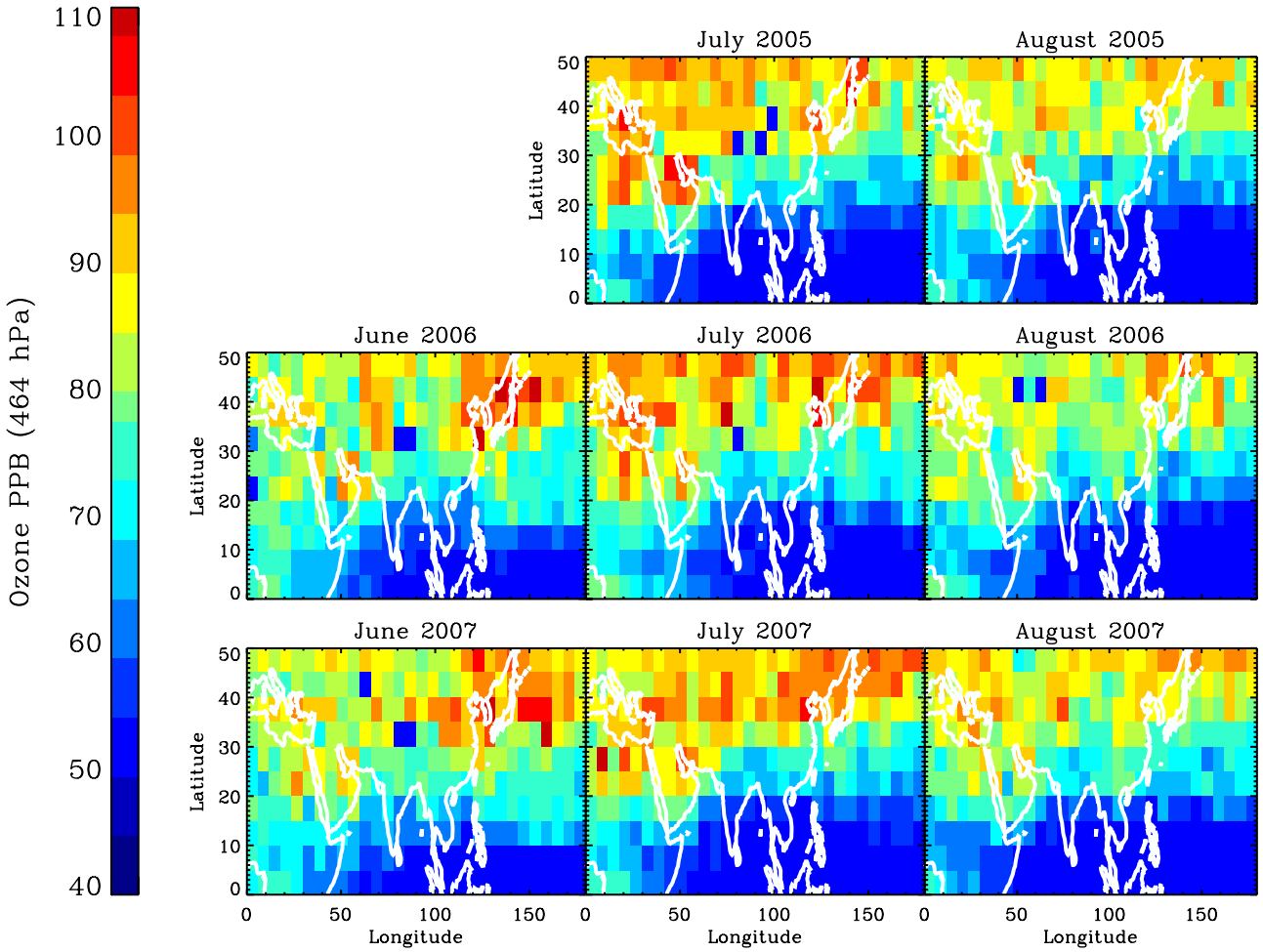

Figure 2. TES monthly averaged ozone at 464 hPa. Data are gridded onto 6° × 6° bins. There are no data for June 2005 as TES was undergoing operational difficulties during that time period. Data are not corrected for the approximately 15% TES bias.

resolution and a priori constraint. Hereafter, we will call this 15% bias the TES bias to distinguish it from the retrieval bias introduced by use of an a priori constraint.

[7] The analysis presented here uses TES data obtained during the summers of 2005, 2006, and 2007, from both the nominal operation mode (the "global survey" mode) and from special observations obtained using the "step-and-stare" mode. The sampling for the global survey mode is one observation every 160 km with 16 orbits per global survey, over a time period of 12 h. The step-and-stare mode spatial sampling is approximately 30 km, but covers only part of an orbit extending 60° in latitude. We use version 3 of the TES data. Only data where the master retrieval quality flag is set to 1 are used. In addition, any data showing a "C" curve are thrown out as discussed in the validation document in the Aura Validation Data Center web site: http://eosweb.larc.nasa.gov/PRODOCS/tes/table_tes.html.

3. TES Ozone Observations

[8] The Asian Monsoon forms in late spring and dissipates in the fall. We therefore focus our analysis on observations in June, July, and August. In this section, we first examine the horizontal distribution of TES monthly averaged observations in the middle and upper troposphere. We then present an analysis of the errors in the data, followed by a comparison of the vertical distribution ozone as observed by TES.

3.1. Horizontal Distribution of TES Ozone in the Middle and Upper Troposphere

[9] The ozone distribution observed by TES at 464 hPa during the summers of 2005, 2006, and 2007 is shown in Figure 2. There are no data for June 2005 since the TES instrument was not operating at that time. All data for which the TES master data quality is set to unity are used. Furthermore, only those data for which the degrees of freedom for signal (DOFS) for the middle troposphere between 300–600 hPa is 0.3 or larger are selected to ensure that the TES retrieval is sensitive to this part of the atmosphere. The grid used for Figure 2 is 6° × 6° and the ozone distribution is constructed by averaging all ozone observations within each grid box. Because of the approximately 6 km vertical resolution of the TES retrieval, the estimated ozone concentration at 464 hPa is influenced by variations in the ozone abundance throughout the free troposphere and lower stratosphere. However, here we show

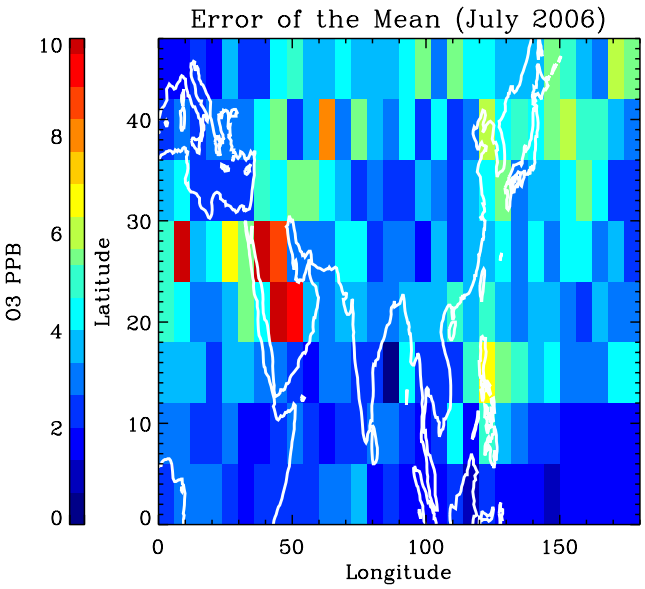

Figure 3a. Standard error of the mean for the July 2006 ozone values at 464 hPa.

the distribution at a single level in the middle troposphere, as opposed to averaging over many pressure levels, because an averaged middle and upper tropospheric quantity would have a latitude dependence due to tropopause variations.

[10] At the 464 hPa pressure level, mean ozone values greater than 90 ppbv are observed over northeast Africa, the eastern Mediterranean, the Middle East, and over Central Asia (north of the Tibetan plateau, between 35°–50°N). We note, however, that we have not corrected for the 10–15% high bias that exists in the TES data (or TES bias) [*H. Worden et al.*, 2007; *Nassar et al.*, 2008] in the middle troposphere when stating this value of 90 ppbv. High ozone abundances are also observed over East Asia but that is the subject for other analysis. This observed spatial distribution of ozone is persistent from year to year, with July typically showing the most enhanced values over northeast Africa and Saudi Arabia. During the 3 years of observations, the ozone abundances over northeast Africa and Saudi Arabia were highest in July 2005. However, as discussed in the section 3.2, many of the grid points over the Middle East shown in Figure 2 had only one or two observations in July 2006 and 2007. Consequently, the year-to-year differences observed over the Middle East may not be robust. Typically, the number of observations in each grid point ranged from 3 to 30.

[11] The spatial distribution of ozone shown in Figure 2 is different from that of the total tropospheric ozone abundances measured by the GOME instrument. In particular, the total ozone abundances from GOME show enhanced ozone abundances across the subtropics of the northern hemisphere in summer [*Liu et al.*, 2006], whereas TES data show more localized enhancements. However, *Liu et al.* [2006] do show peak total tropospheric ozone columns over the Eastern Mediterranean and northwestern Saudi Arabia, which is somewhat consistent with the ozone distribution measured by TES. Differences between the two ozone measurements are likely due to differences in the sensitivity of the instruments to tropospheric ozone, sampling, and the retrieval approach.

3.2. Sensitivity and Errors of TES Ozone Estimates

[12] The sensitivity of the TES ozone retrievals to the true atmospheric ozone abundance depends primarily on atmospheric temperature, clouds, and trace gas amounts. As these quantities are strongly influenced by the summertime Asian monsoon, it is necessary to determine how their variability impacts the TES retrievals in this region. In this section we examine the errors, sensitivity, and bias of the TES ozone retrievals to show that the enhancements in the observed spatial distribution of ozone is larger than the errors. For brevity we limit the error characterization to the ozone values of July 2006 as we do not find a significant difference in the error characterization from month to month and season to season.

[13] The total error for each TES ozone observation is a function of the noise of the satellite measurement, atmospheric temperature, clouds, and the effects of interfering species such as water [e.g., *Worden et al.*, 2004]. These errors are either random or weakly correlated so that, for the case of the mean values in Figure 2, we can effectively average them for the collection of measurements in each grid box. This error is called the observation error in the TES data product files. Typical values for the observation error for the altitude shown in Figure 2 are 3–7%. The error of the average of several profiles is substantially smaller than the observed variability of ozone within the grid box which can range from 15 to 30%.

[14] The random uncertainty of the mean ozone values shown in Figure 2 is therefore due primarily to ozone variations within each grid box. This uncertainty is simply the standard error of the mean. The standard error on the mean values shown in Figure 2 can in principle be theoretically calculated by averaging over the expected random errors for the distribution of retrievals in each grid box. However, this approach assumes that the statistics of the atmosphere in the region of interest are well known, which may not be a good assumption for the region affected by the summertime Asian monsoon, given the scarcity of ozone profile observations in this region. We can empirically calculate the error on the mean by dividing the root mean square (RMS) of the ozone values within each grid point by the square root of the number of observations in each grid [*J. Worden et al.*, 2007]. As seen in Figure 3a, the error on the mean for July 2006 is typically 5 ppbv or less for the regions with the largest ozone values, but can be higher over parts of Central Asia because of the larger variance over this region. The topography in this region can also make atmospheric retrievals more challenging, which limits the number of available ozone profile estimates within some of the grid boxes, thereby increasing the error of the mean. In particular the error on the mean is large over parts of Saudi Arabia because of limited (one to two) observations per grid box for the July 2006 (and also July 2007, not shown).

[15] The TES estimates of tropospheric ozone, or any other trace gas, are dependent on the sensitivity of the retrievals to the true atmospheric abundance of ozone as well as to the a priori constraint used for the retrieval. Limitations in the sensitivity of the TES retrieval to the true atmospheric ozone abundance therefore provide another

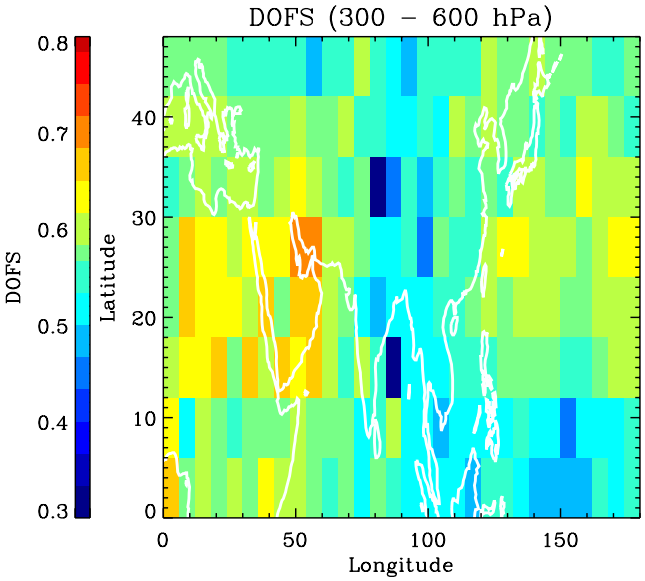

Figure 3b. DOFS for the region between 300 and 600 hPa.

source of error that can influence our conclusions about the observed ozone distribution. This dependency of the retrieval on the a priori is represented by the following equation:

$$\hat{\mathbf{x}} = \mathbf{x_a} + \mathbf{A}(\mathbf{x} - \mathbf{x_a}) \tag{1}$$

where $\hat{\mathbf{x}}$, in this case, is the TES ozone profile estimate. The a priori constraint is given by $\mathbf{x_a}$. The true ozone distribution is given by $\mathbf{x}$ and the sensitivity of the estimate to this ozone is given by the averaging kernel matrix, $\mathbf{A} = \frac{\partial \hat{\mathbf{x}}}{\partial \mathbf{x}}$. The quantities $\mathbf{x}$, $\hat{\mathbf{x}}$, and $\mathbf{x}_a$ are expressed in terms of the natural logarithm of the volume mixing ratio of ozone. The TES ozone estimate, a priori constraint, averaging kernel matrix, and the various error covariances are provided with all TES observations. The averaging kernel is a function of the sensitivity of the TES measured radiance to the distribution of ozone, the noise in the radiance, and the constraint matrix used to regularize the retrieval. For ozone, the constraints and constraint matrices are computed using ozone fields simulated by the MOZART global chemistry and transport model (CTM) binned into a 60° longitude by 10° latitude bins [*Worden et al.*, 2004].

[16] As seen in equation (1), TES estimates are biased toward the a priori constraint computed from the MOZART model. This retrieval bias is separate from the 10–15% observed TES bias that is due to either instrumental or spectroscopic uncertainties. We examine here to what extent variations in the a priori constraint influences our conclusions about the observed ozone variations. The bias in the TES estimates from the a priori constraint is given by the difference between the true ozone distribution and the TES estimate of this true distribution:

$$\hat{\mathbf{x}} - \mathbf{x} = (\mathbf{I} - \mathbf{A})(\mathbf{x_a} - \mathbf{x}), \tag{2}$$

A useful metric for the sensitivity of the ozone estimate to the true atmospheric abundance of ozone is the DOFS which is the sum of the diagonal elements of the averaging kernel matrix; the diagonal element of the averaging kernel matrix describes the sensitivity of the ozone estimate for the corresponding pressure level to the true distribution of ozone at that pressure level. In order to determine if the ozone estimates shown in Figure 2 are sensitive to the true distribution, we examine the average DOFS for the altitude region between 300–600 hPa. As shown in Figure 3b, for the geographical and altitude region of interest there is, on average, 0.65 DOFS. Consequently, while the estimate is sensitive to the true distribution of ozone in this region, it is useful to determine the extent to which the retrieval bias might contribute to the spatial variability in the ozone retrievals.

[17] An approach for estimating an upper bound on the retrieval bias is to replace the "true state" ozone ($\mathbf{x}$) on the right side of equation (2), with some value that is unlikely, although not unphysical. For this sensitivity test we selected an a priori constraint from a retrieval over the clean Pacific Ocean, at approximately 30°N and 180°W. Ozone values in this a priori profile are 30–40 ppbv in the lower troposphere and 40–50 ppbv in the upper troposphere. Note that this linear operation is equivalent to calculating a different estimate by swapping in a fixed a priori constraint [*Rodgers and Connor*, 2003].

$$\hat{\mathbf{x}}_2 = \hat{\mathbf{x}}_1 + (\mathbf{I} - \mathbf{A})\left(\mathbf{x}_a^2 - \mathbf{x}_a^1\right) \tag{3}$$

where $\hat{\mathbf{x}}_1$ is the original TES ozone estimate and $\hat{\mathbf{x}}_2$ is the new TES ozone estimate, $\mathbf{x}_a^1$ is the constraint used for the original TES ozone retrieval, and $\mathbf{x}_a^2$ is the fixed constraint used to change the TES estimate. The expression $(\mathbf{I} - \mathbf{A})(\mathbf{x}_a^2 - \mathbf{x}_a^1)$ is now equivalent to the right hand side of equation (2) if we replace the true ozone distribution with this new constraint in order to estimate an upper bound on the bias from the constraint vector.

[18] We first recalculate the ozone estimate assuming a fixed a priori constraint vector [*Kulawik et al.*, 2008]. This new estimate is shown in Figure 3c for the July 2006 monthly mean. Over the Sahara and Middle East, between 20 and 30 degrees latitudes, differences between the two

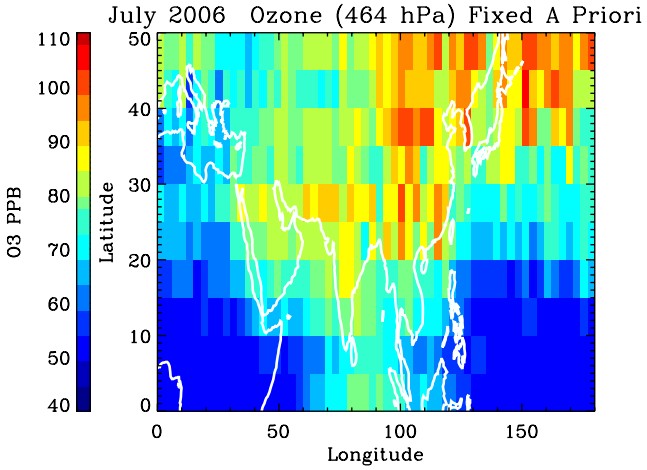

Figure 3c. TES estimate of ozone at 464 hPa if we use a fixed a priori constraint vector.

estimates are approximately 10 ppbv. Over Northeast Africa, the Eastern Mediterranean, and north of the Tibetan plateau differences are approximately 5 ppbv between the two ozone estimates. The larger differences of 10 ppbv result because the tropopause in the fixed prior is near 250 hPa whereas the tropopause over the Sahara and the Middle East is near 100 hPa.

[19] However, comparison of the two estimates (between Figure 2 (middle) and Figure 3c) shows little change in the relative spatial variability of ozone over this region. We can therefore conclude that variations in the a priori constraint does not affect our conclusions about the spatial variability of ozone over this expansive region. Note that a bias from the a priori constraint is removed when comparing to ozonesondes or a model because these profiles are first transformed using equation (1) before comparing to TES observations [*H. Worden et al.*, 2007]. For the same reason, TES data assimilated into a model where the model is first transformed using equation (1) will also remove the effects of the a priori constraint.

3.3. Comparisons to MOZAIC Data

[20] As noted earlier, comparison of TES tropospheric ozone profiles to ozonesondes show that the TES ozone estimates are biased high in the middle troposphere by between 10 and 15% [*H. Worden et al.*, 2007; *Nassar et al.*, 2008]. This TES bias is possibly due to unquantified calibration errors, spectroscopic errors, or some other unknown effect. Unfortunately, there are few ozonesonde measurements over North Africa, the Middle East, and Asia with which to compare the TES data to ensure that the bias observed in other parts of the world is appropriate for this region. For this reason, we compare ozone climatologies derived from MOZAIC to climatologies derived from the TES data. We use monthly mean ozone climatologies generated from MOZAIC data between 1996 and 2005 because there are no specific coincidences between these measurements and the TES data. These climatologies are generated for the cities of Dubai, Teheran, and Delhi. We note that a significant challenge with this comparison is that the MOZAIC climatologies are representative of a region that is much smaller than can be consistently sampled by TES. For this reason the TES climatologies are generated by accumulating profiles for summer of 2005, 2006, and 2007 over $5^\circ \times 5^\circ$ bins centered about the cities of Dubai, Teheran, and Delhi.

[21] The precision of the MOZAIC ozone data is 2 ppbv and the sensors are calibrated every 500 flights hours [*Thouret et al.*, 1998a]. The number of profiles used to calculate the monthly means range from 47 to 110. The constructed climatologies from these profiles are consistent with those based on ozonesondes [*Thouret et al.*, 1998b].

[22] A second major challenge in comparing the TES and MOZAIC profiles is that we cannot accurately account for the smoothing influence of the TES vertical resolution and the bias introduced by the a priori constraint because of the error introduced by truncating the TES profile at approximately 200 hPa, the upper limit of the MOZAIC profiles. This truncation introduces a ''cross-state'' error [*Worden et al.*, 2004] that is due to uncertainties in the TES estimated ozone in the upper troposphere and lower stratosphere. This cross-state error is largest at 200 hPa and becomes smaller at higher pressures. Taking into account the lower sensitivity to ozone of the TES estimates for pressures above 800 hPa, the most useful comparison between the TES and MOZAIC data will be between 300–700 hPa. For this reason we average the ozone values from both the TES and the MOZAIC data between 300–700 hPa for this comparison. These TES averages, and the standard error of the mean (for the averages) are shown with the corresponding averages for MOZAIC in Figure 4. The TES ozone values have been decreased by 12% to account for the 10–15% known bias. Despite the temporal and spatial sampling differences between the TES and MOZAIC data, the agreement is within the standard error of the mean for most of the TES data. In addition, both the TES and MOZAIC data show similar month-to-month changes in the climatology with the exception of June over Teheran. We therefore conclude that the TES data are likely biased high in these regions by 10–15% as observed elsewhere in the world with ozonesonde data.

3.4. Vertical Distribution of TES Ozone Observations

3.4.1. Vertical Distribution of Ozone over India, the Tibetan Plateau, and Central Asia

[23] Having established the summertime horizontal distribution of ozone across North Africa and Asia, we now examine the vertical distribution of ozone over this region using TES observations. Characterizing the vertical distribution of ozone is necessary for understanding how surface emissions, deep convective transport, long-range transport of pollution, and NOx production from lightning influence tropospheric ozone abundances during this period.

[24] Figure 5 shows the vertical distribution of ozone as observed by TES between 70°–90°E and 20°–50°N (the region covering India, the Tibetan Plateau, and Central Asia). All data have been interpolated to a latitudinal grid of 0.5 degrees. We choose a finer latitudinal spacing than that used in Figure 2 because the coarser longitudinal spacing allows for more data to be used in Figure 5. The average surface pressure over this 20° longitudinal swath is shown as a white line on the bottom. The surface pressure changes in each plot because of the different sampling in each month of observations. The dashed line represents the pressure at 464 hPa for comparison of these vertical distributions with Figure 2. Only profiles where the DOFS in the middle troposphere (300–600 hPa) are larger than 0.3 are selected to ensure sensitivity of the TES estimates to variations in tropospheric ozone at these altitudes.

[25] The vertical distribution of ozone shown in Figure 5 is characterized by enhanced abundances of ozone, with values that can exceed 100 ppbv at approximately 300 hPa between 25° and 40°N. This enhanced layer of ozone is present in June and July and begins to dissipate by August. The enhanced layer is not apparent in Figure 2 because it is at higher altitudes than the 464 hPa pressure level shown in Figure 2. The lower ozone amounts of approximately 60–70 ppbv at 200 hPa, between 20° and 30°N, during July and August are consistent with AIRS ozone observations shown by *Randel and Park* [2006].

[26] An additional test to determine the altitude location of the enhanced ozone in this region is to use a fixed a priori constraint, following the approach discussed in section 3.2. Vertical ozone distributions from TES using a fixed a priori

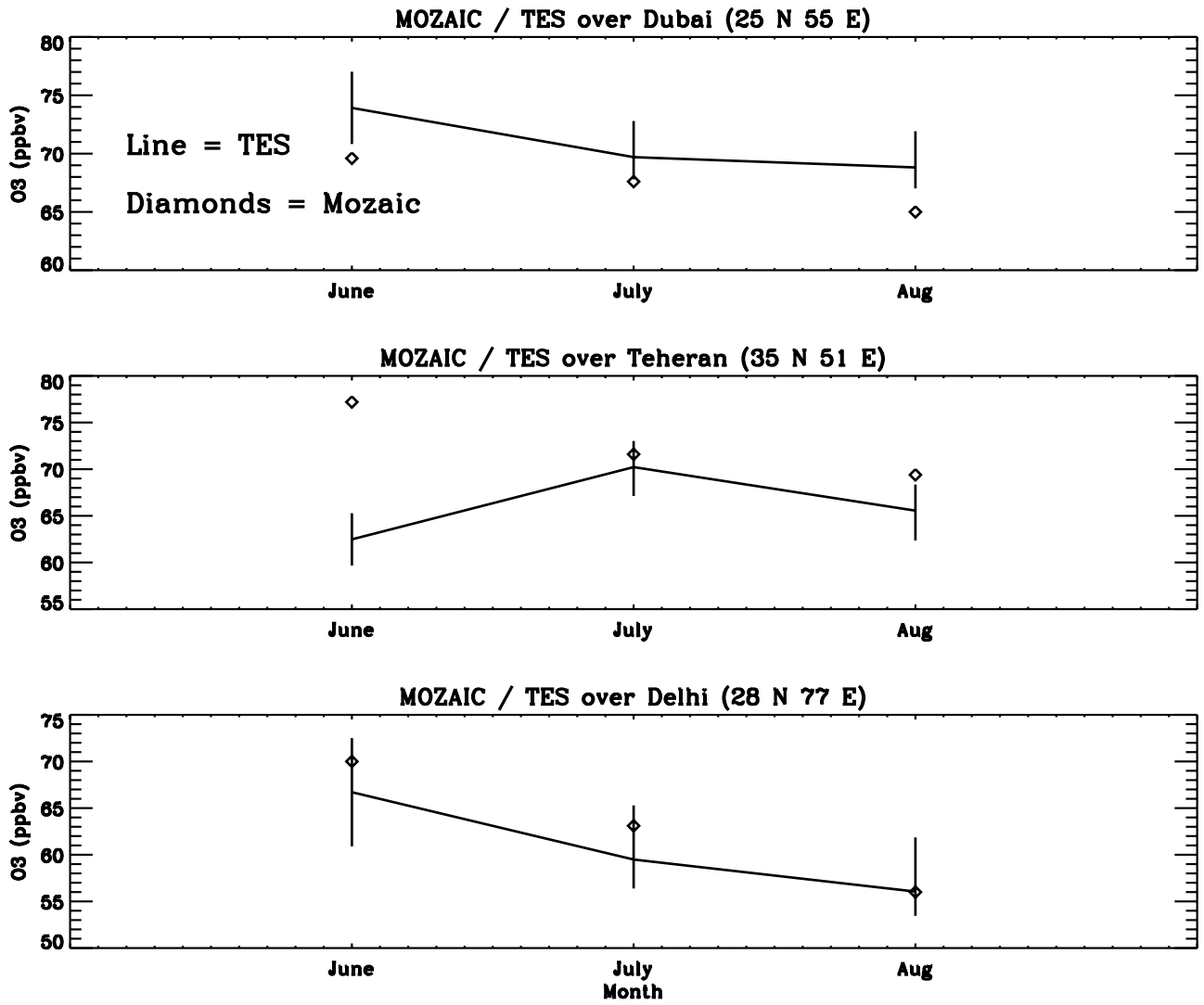

Figure 4. Comparison between 10-year climatologies derived from MOZAIC ozone measurements and a 3-year climatology derived from TES ozone observations. The error bars are the standard error on the mean for the TES ozone measurements. The TES ozone values have been decreased by 12% to account for the 10–15% TES bias.

constraint vector are shown in Figure 6. The vertical distributions for June show slight changes. However, the differences in the vertical distributions of ozone using a fixed a priori constraint do not change our conclusion about ozone enhancements near 300 hPa for latitudes between 20° and 40°N for July and August.

[27] Another feature present in the TES ozone data is the region of ozone abundances larger than 150 ppbv North of 40°N at pressures less than 300 hPa. Because the coarse 20° longitudinal gridding used to create Figure 6 might obscure the vertical variations of the ozone, we therefore show in Figure 7 special observations from TES that have a 35 km spacing between consecutive observations as opposed to the 160 km spacing between observations in the TES global survey data used in Figure 5. These special observations are part of a yearly set of observations used to study boreal fires and Asian pollution. As with the vertical distributions shown in Figure 5, ozone abundances of about 100 ppbv at 300 hPa are observed near 30°N. However, significantly higher ozone concentrations, between 150 ppbv to 200 ppbv, are observed north of 35°N in the upper troposphere. Between 35° and 45°N, the total error of these ozone estimates range from 15% to 30%, with a mean error of about 23%. However, north of 45°N, the total error of the observed ozone at 300 hPa is typically 17%. The range of uncertainties gives confidence that the observed ozone amounts are not due to interference between the stratosphere and troposphere in the TES ozone retrieval.

[28] Enhanced ozone in this region is consistent with global analyses of thermal, dynamical and chemical definitions of the tropopause by *Stajner et al.* [2008]. They showed that during July 2005 the sensitivity of the tropospheric ozone column to the choice of the tropopause definition is the largest in this region. Ozone attains 100 ppbv at altitudes lower than the altitudes of a thermally or dynamically defined tropopause.

[29] This region of high ozone abundances is also colocated with TES observations of low upper tropospheric

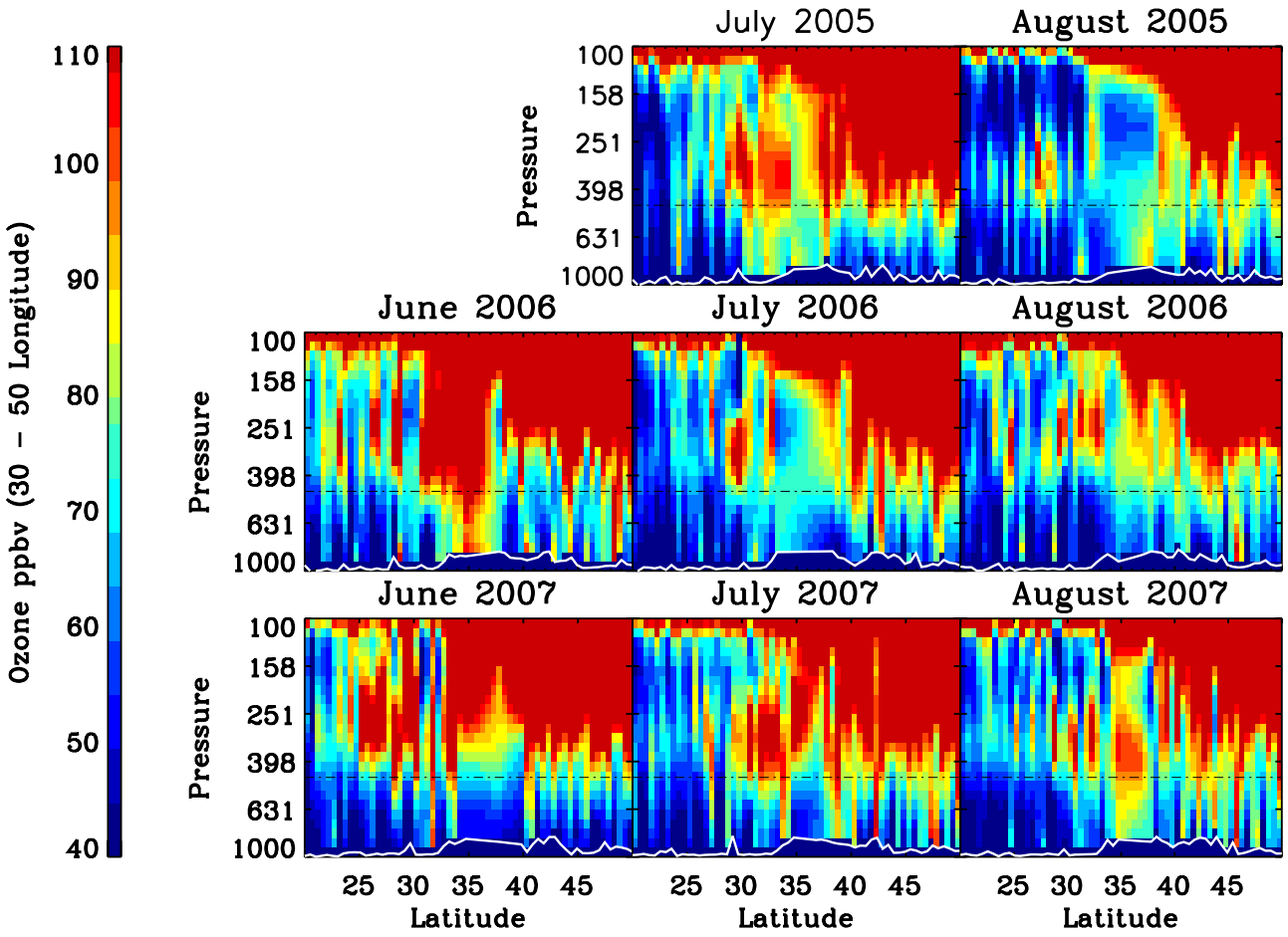

Figure 5. TES vertical ozone distributions during the summers of 2005, 2006, and 2007 for longitudes between 70° and 90°E. The vertical scale is the log of pressure. The dashed line indicates the 464 hPa level for comparison with Figure 2. The bottom white line shows the average surface pressure for the set of observations during the specified time period and latitude/longitude range. Data are not corrected for the approximately 15% TES bias.

water (not shown) and the westerly jet, which, as shown by *Randel and Park* [2006], is associated with subsiding air. The high ozone and low water suggest a stratospheric origin which is consistent with of the analysis of *Moore and Semple* [2005], who found that ozone at the surface in this region can originate from the stratosphere. They are also consistent with the analysis of *Sprenger and Wernli* [2003] who examined 15 years of ERA15 meteorological data from the European Center for Medium-Range Weather Forecasting and found that stratosphere to troposphere exchange is at a maximum over central Asia in summer. *Ding and Wang* [2006] also suggested that stratospheric intrusions were primarily responsible for enhanced surface ozone abundances observed over the Tibetan Plateau. Other TES step and stares taken during the summer of this same region show similar behavior but are not shown because they had significant data gaps because of clouds and increased retrieval failure rate over the mountain regions.

3.4.2. Vertical Distribution of Ozone Over the Middle East

[30] The vertical distribution of ozone between 20° and 50°N, averaged between 30° and 70°E and between 20° and 50°E are shown in Figures 8 and 9, respectively. Both Figures 8 and 9 show enhanced ozone abundances of about 100 ppbv in the middle or upper troposphere. The major difference between the ozone distributions in Figures 8 and 9 and those in Figure 5 (over India and Tibet) are that the peak ozone amounts for latitudes equatorward of 30°N are at lower altitudes (particularly over northeast Africa and Saudi Arabia in Figure 9), as indicated by the dashed line at 450 hPa. For latitudes poleward of 30°N, high ozone abundances are located at higher altitudes, near 300 hPa. For brevity, we do not show ozone amounts using a fixed a priori constraint although we note that our conclusions about the vertical distribution of ozone would not change using a fixed prior.

3.5. Assimilation of TES, OMI, and MLS Data

[31] As discussed above, conducting a direct quantitative comparison between the TES, MOZAIC, and MLS data is challenging because of the lack of spatiotemporal coincidence between the data sets and the fact that MLS and MOZAIC do not provide complete vertical profiles of ozone. In this section we therefore indirectly compare the TES and MLS data through assimilation of the data into the GEOS-Chem model and the GMAO Goddard Earth

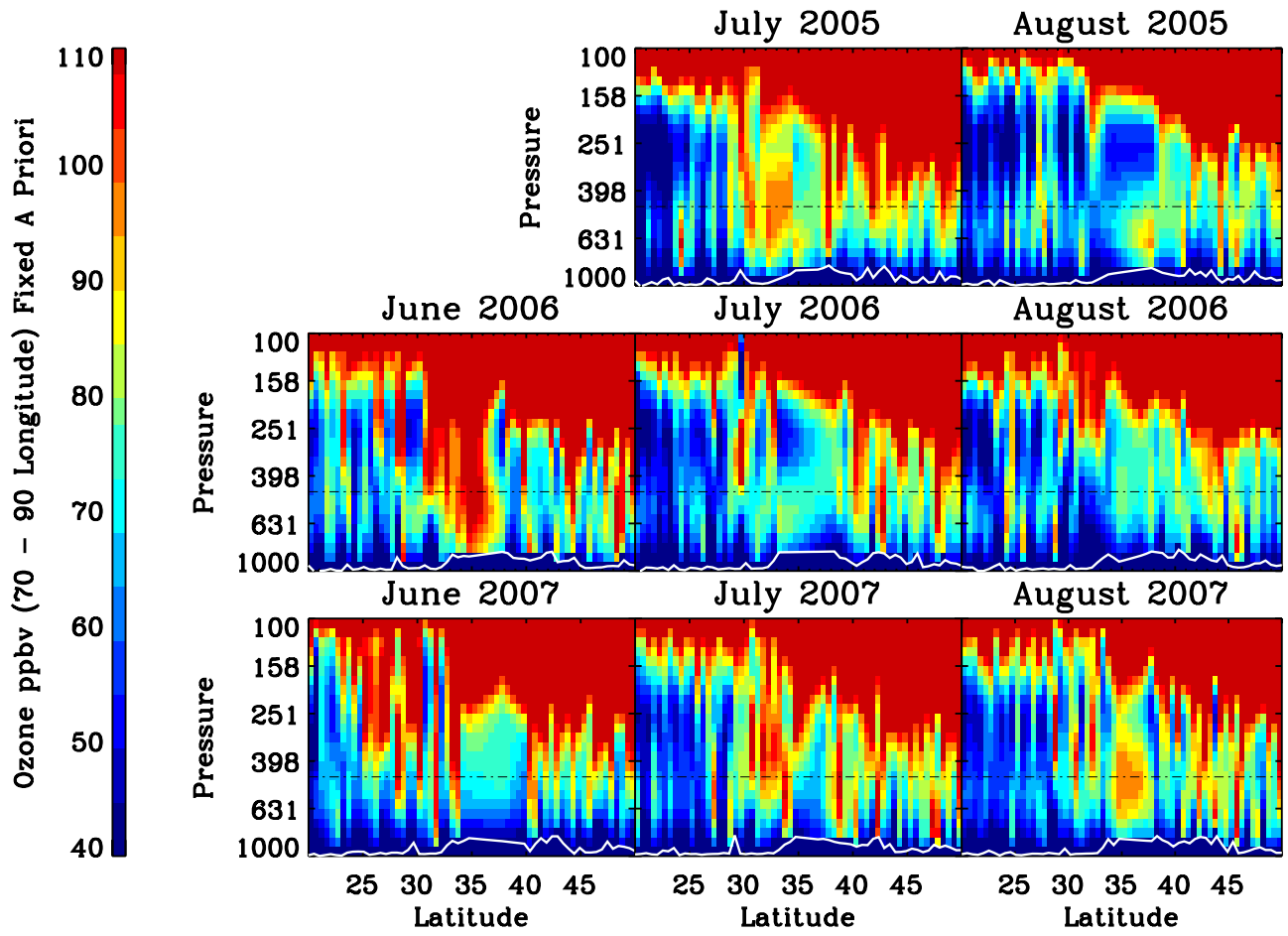

Figure 6. Same as in Figure 5 except the ozone profiles have been recalculated using a fixed a priori constraint.

Observing System (GEOS-4) general circulation model (GCM). This enables us to assess the consistency of the information that the data sets provide on the distribution of ozone when they are assimilated into the models. Recently, *Parrington et al.* [2008] assimilated TES observations of ozone into the GEOS-Chem model and *Stajner et al.* [2008] assimilated data from MLS and OMI into the assimilation system at GMAO. Details of the models and the assimilation systems are described in the Appendix.

[32] The distribution of ozone in the upper troposphere produced by the GEOS-Chem model with and without assimilation of TES data is compared with that obtained from assimilation of OMI and MLS data (henceforth referred to as OMI+MLS) in Figure 10. The GEOS-Chem model without assimilation overestimates ozone in the Middle East, whereas it underestimates ozone across much of the northern hemisphere, relative to OMI+MLS. *Hudman et al.* [2007] and *Parrington et al.* [2008] attributed the underestimate of ozone in the upper troposphere in GEOS-Chem to an underestimate of lightning-produced NOx in this version of the model. Assimilation of TES data into the model reduces this low bias from a mean of 6.8 ppb to 1.4 ppb over North Africa, the Middle East, and Asia. As shown in Figure 10d, the distribution of ozone differences between the models is less skewed and more sharply peaked following assimilation of TES data into GEOS-Chem. Note that, as explained in the Appendix, the bias in the TES ozone data as reported by *Nassar et al.* [2008] was removed during assimilation of the data into GEOS-Chem.

[33] The vertical profiles of ozone at four selected locations across western and central Asia are shown in Figure 11. Assimilation of TES data into GEOS-Chem results in significantly improved agreement between the GEOS-Chem and the OMI+MLS profiles, suggesting that the information on the vertical structure of ozone offered by the TES data in the upper troposphere is consistent with that provided MLS. Note that since the MLS data do not extend down to altitudes below 215 hPa, the OMI+MLS assimilation does not constrain the vertical structure of ozone in the lower and middle troposphere. This may explain some of the discrepancies in the lower troposphere between the TES and OMI+MLS assimilated profiles in Figure 11.

[34] The monthly mean vertical distribution of ozone along 45°E and 70°E is shown in Figure 12. Without assimilation of TES data into GEOS-Chem, the model places the ozone tropopause too low in the subtropics (between 20° and 30°N) and too high in the extratropics (40°–50°N), relative to OMI+MLS. After assimilation of TES data into GEOS-Chem, there is excellent agreement in the structure of the ozone tropopause in the two models. In

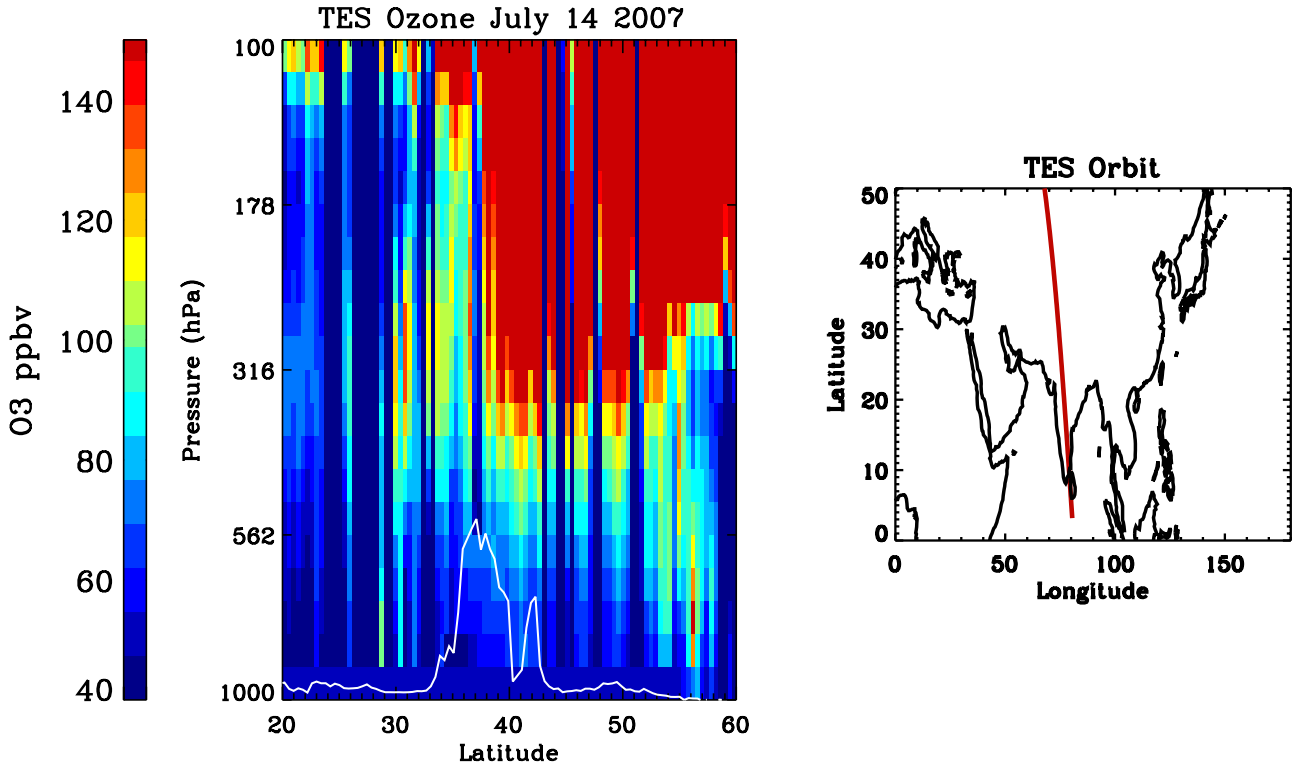

Figure 7. TES ozone profiles from the "step and stare" mode. There is approximately 1 observation every 35 km. The white line is the average surface pressure. Data are not corrected for the approximately 15% TES bias.

the middle troposphere over the Middle East (along 45°E and between 20° and 30°N) ozone abundances in GEOS-Chem are reduced by assimilation of TES data, whereas over central Asia (along 75°E and 35°–45°N) they are enhanced. The changes in ozone over central Asia are particularly striking as the TES assimilation shifted the broad ozone maximum in the upper troposphere in GEOS-Chem from between 25° and 35°N to between 35° and 45°N, producing good agreement between the assimilated ozone distributions.

4. Discussion and Conclusions

[35] We present new observations from the TES instrument of the horizontal and vertical distribution of ozone over North Africa, the Middle East, and Central Asia. Over India, between 20°N and 30°N, high ozone abundances of approximately 100 ppbv are observed at approximately 300 hPa, whereas over the Middle East the enhanced ozone is located near 450 hPa. Lower ozone abundances of about 50 ppbv are observed above and below this layer of enhanced ozone. The region of enhanced ozone abundances over the middle East, near 450 hPa, is consistent with the model predictions from *Li et al.* [2001]. Over Central Asia, TES observes high abundances of ozone, exceeding 150 ppbv, at pressures of approximately 300 hPa. These high ozone levels are colocated with the westerly jet and are indicative of mixing between the stratosphere and troposphere; further analysis is needed verify the source of this ozone.

[36] The TES observations of tropospheric ozone are corroborated by MOZAIC summertime ozone climatologies over Tehran, Dubai, and Delhi for pressures between 300 hPa and 700 hPa. After accounting for the TES middle tropospheric bias of 10–15%, we find that the TES data typically agree with the MOZAIC climatology within the standard error on the mean of the TES measurements. Assimilation of TES data into the GEOS-Chem model produces a distribution of ozone over North Africa, the Middle East, and Asia which is in good agreement with that obtained by assimilation of MLS and OMI data into the GMAO GEOS-4 assimilation system. Across the region, at 7–8 km, the bias between GEOS-Chem and the assimilated OMI and MLS fields is reduced from 6.8 ppbv to 1.4 ppbv following assimilation of TES data.

[37] Previous observations of tropospheric and stratospheric trace gases in the Asian Monsoon region revealed a complex system involving deep convective transport of boundary layer air to the upper troposphere followed by entrainment into the strong westerly and easterly winds in the subtropics and tropics, respectively. TES observations of the vertical and horizontal distribution of tropospheric ozone provide a more detailed description of the distribution of tropospheric ozone, which will enable us to better understand how the chemical and dynamical processes in the Asian monsoon region impacts tropospheric ozone. *Liu et al.* [2009], for example, recently used TES data to quantify the contribution of long-range transport of pollution and local photochemistry to the summertime buildup of ozone over the Middle East. In subsequent studies, we will

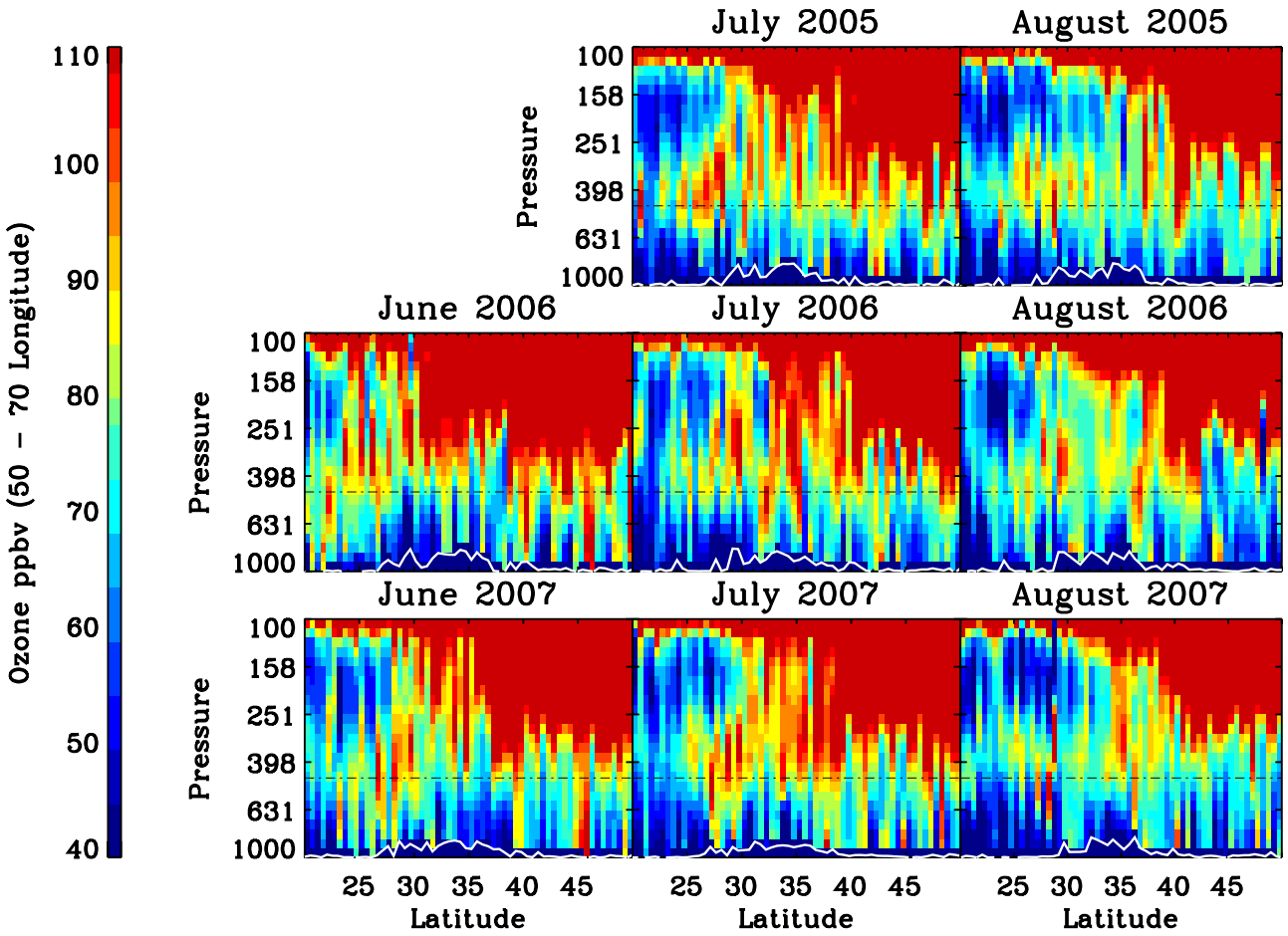

Figure 8. TES observed vertical ozone distributions for longitudes between 50° and 70°E. The white line indicates the average surface pressure. Data are not corrected for the approximately 15% TES bias.

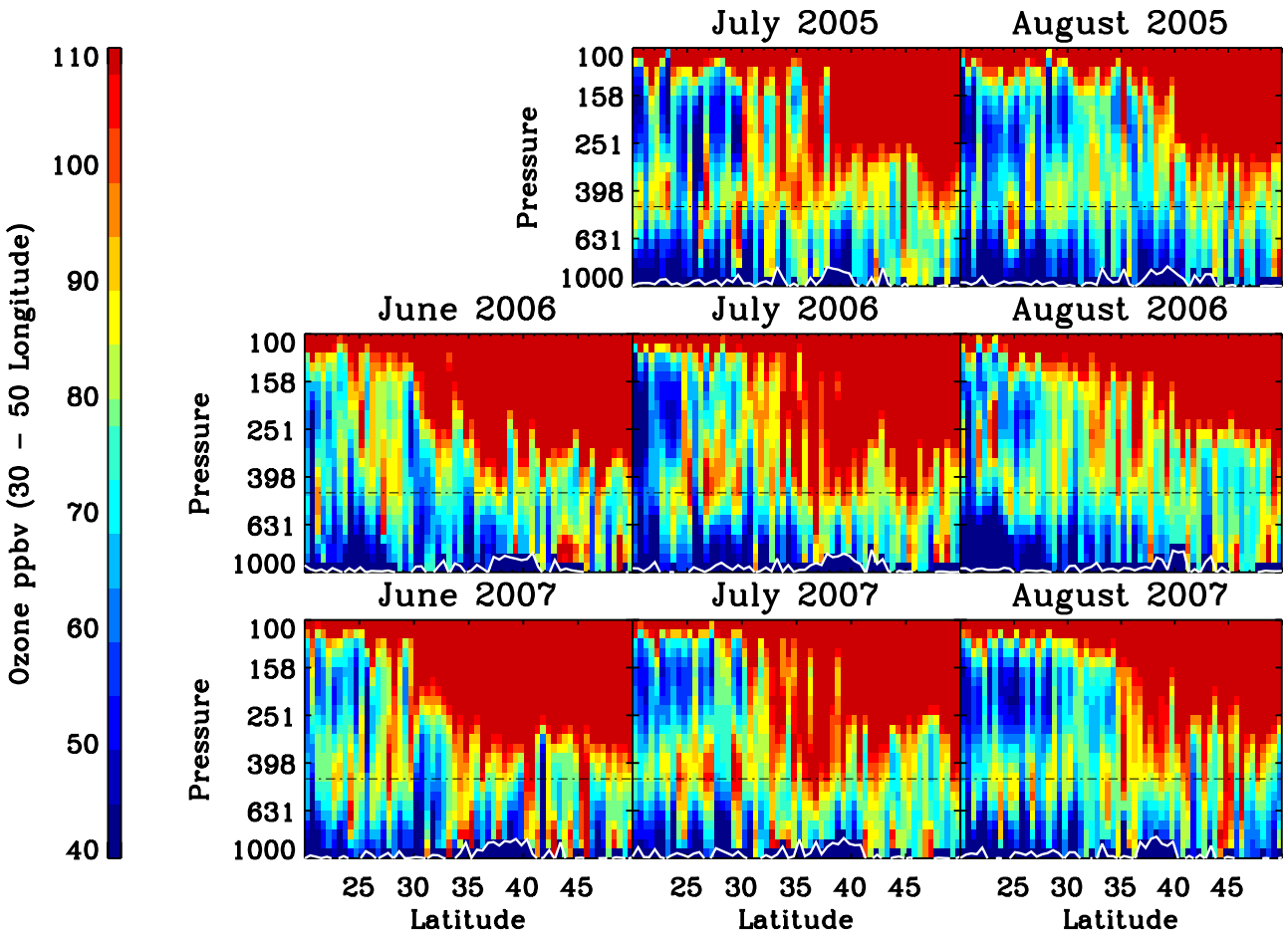

Figure 9. TES observed vertical ozone distributions for longitudes between 30° and 50°E. The white line indicates the average surface pressure. Data are not corrected for the approximately 15% TES bias.

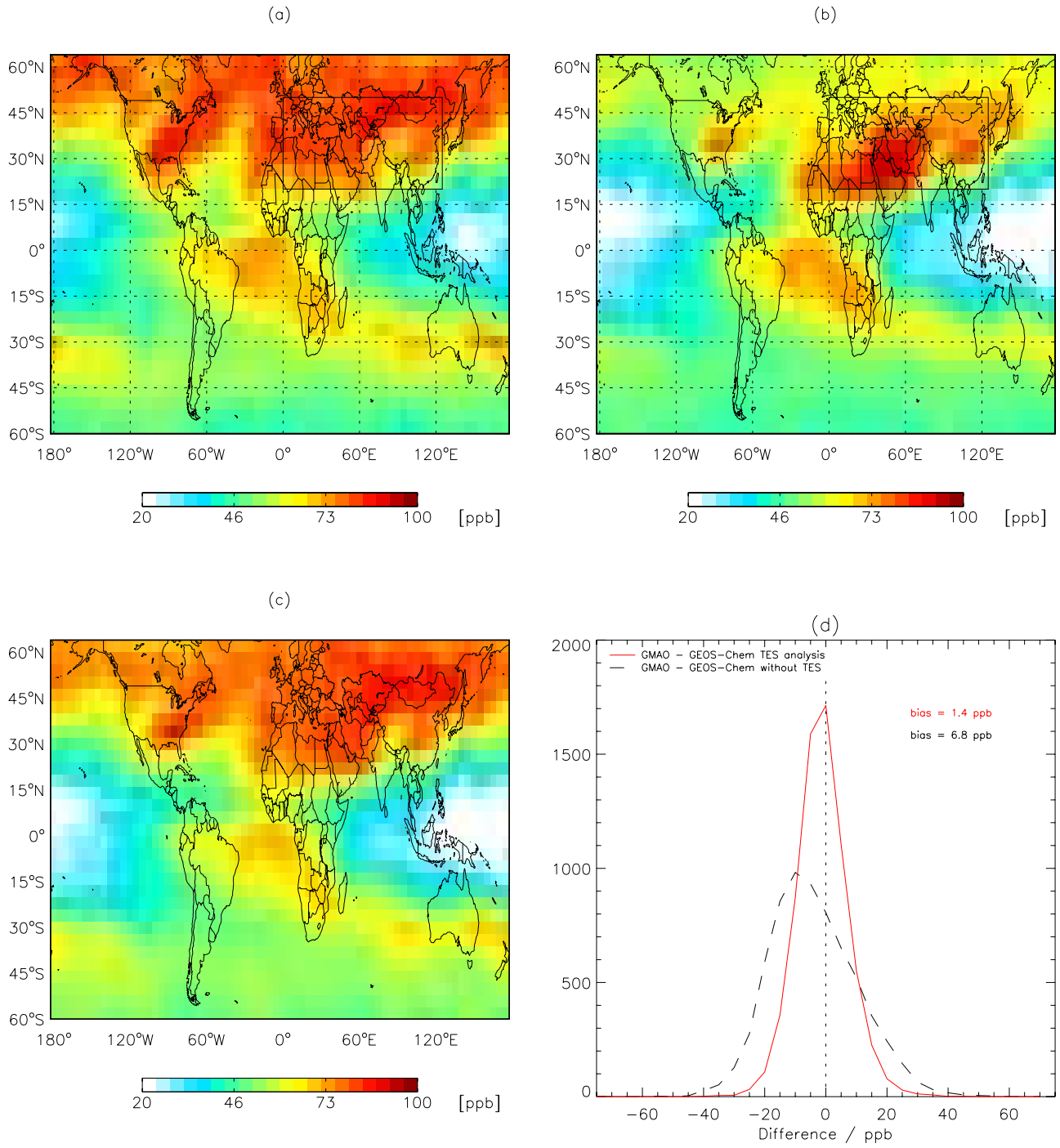

Figure 10. Mean August 2006 ozone distribution at 7–8 km produced by (a) assimilation of OMI and MLS data into the GMAO GEOS-4 GCM, (b) the GEOS-Chem model, and (c) the GEOS-Chem model after assimilation of bias-corrected TES data following *Nassar et al.* [2008]. (d) Histogram of the differences in ozone between the GMAO ozone assimilation and the GEOS-Chem model with (red line) and without (black dashed line) assimilation of TES data. The ozone differences were calculated over the region indicated by the box in Figures 10a and 10b and are based on daily modeled fields at 0 GMT.

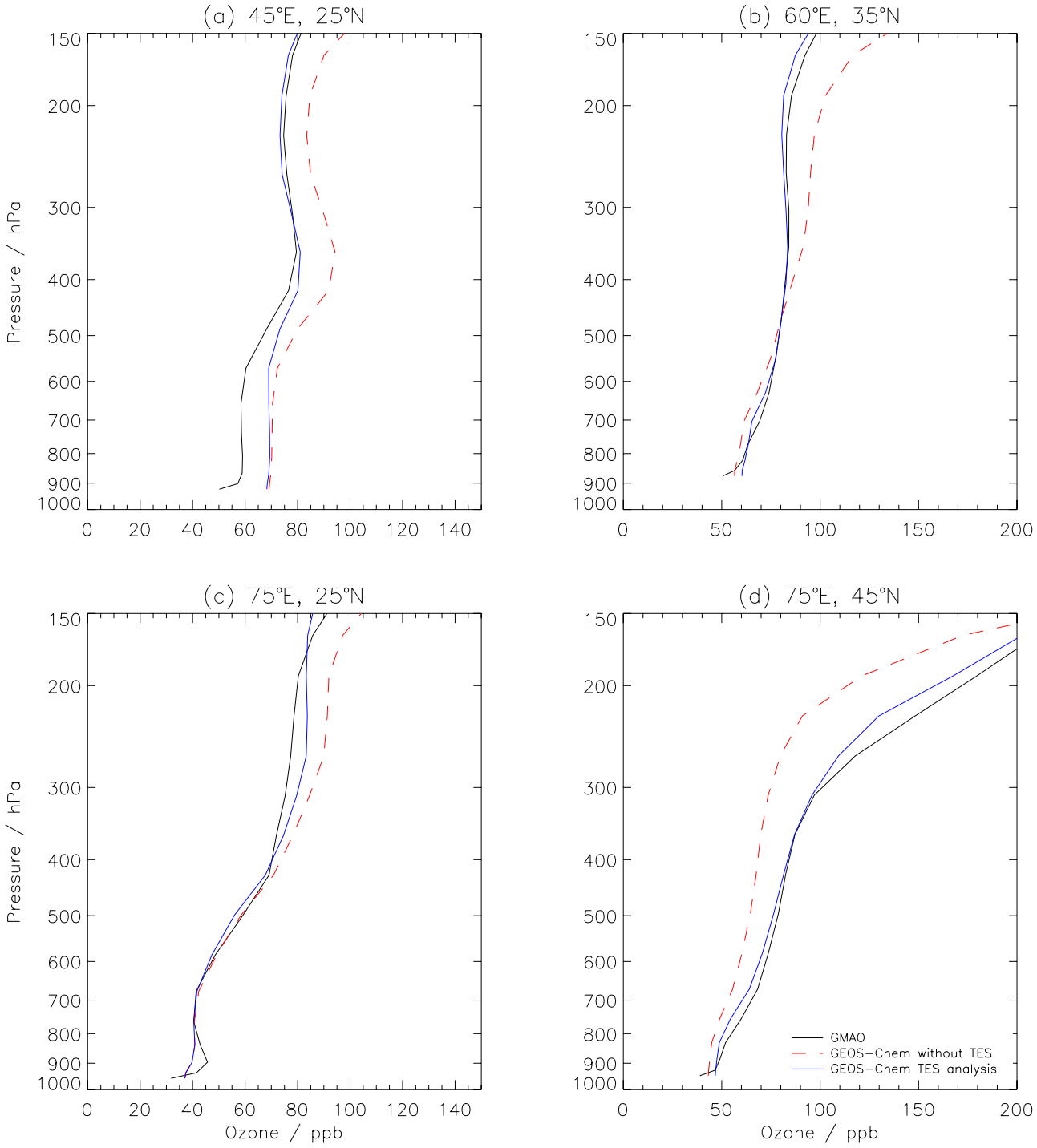

Figure 11. Comparison mean modeled profiles across the Middle East and Asia for August 2006. The black line shows the profiles from the assimilation of OMI and MLS ozone data into the GMAO GEOS-4 GCM, the blue line indicates the profiles from the assimilation of TES ozone data into the GEOS-Chem model, and the red dotted lines are the GEOS-Chem profiles obtained without assimilation of TES data.

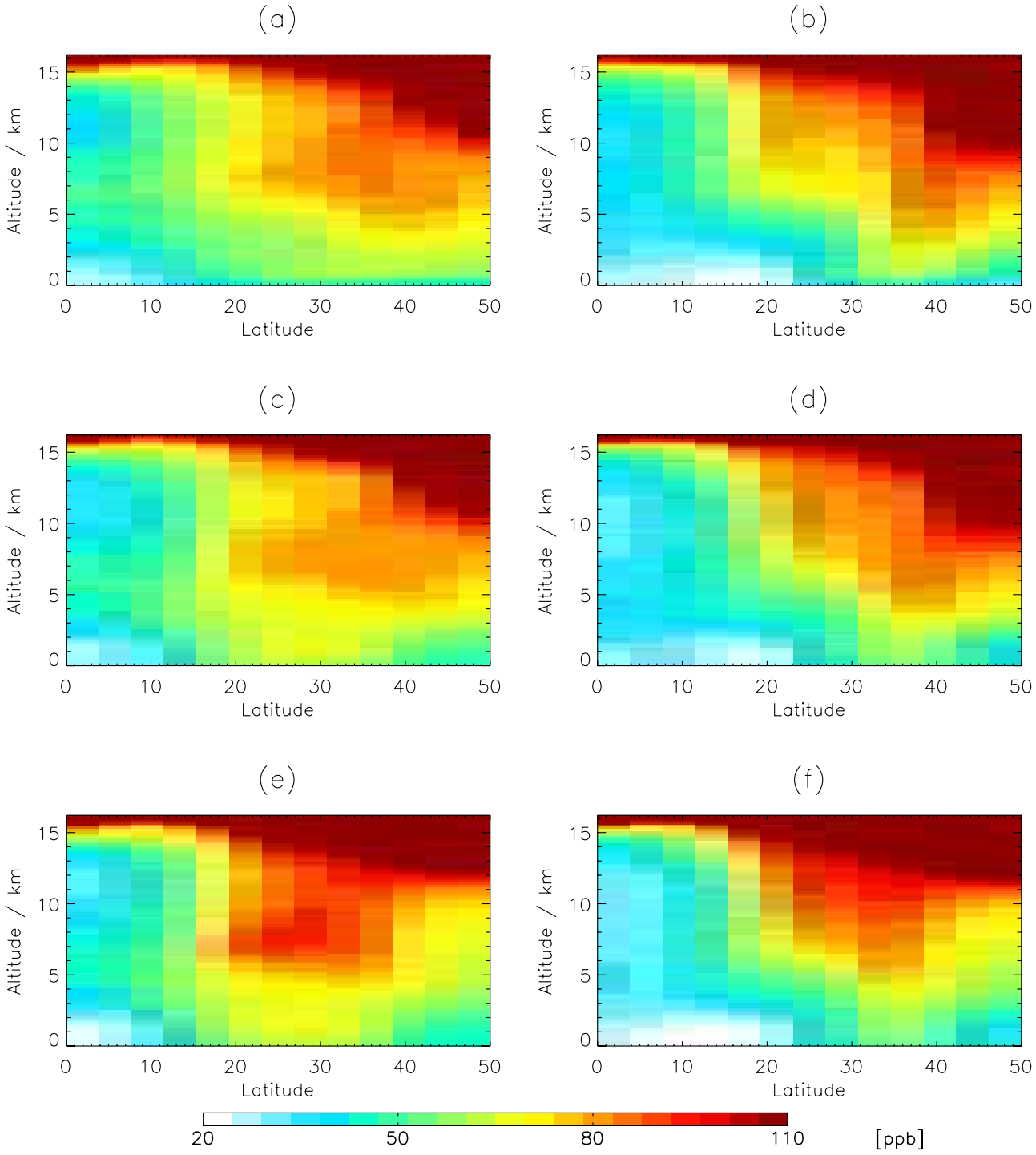

Figure 12. Monthly mean altitude-latitude cross sections of modeled ozone abundances for August 2006 along (left) 45°E and (right) 70°E for (a)–(b) the GEOS-4 GCM with assimilated observations from OMI and MLS, (c)–(d) the GEOS-Chem model with assimilated data from TES, and (e)–(f) the GEOS-Chem model without assimilation of TES data.

focus on understanding the processes responsible for the ozone distribution over South Asia. TES observations are providing valuable new information about the distribution of ozone in the middle troposphere in this relatively data sparse region of the globe.

Appendix A: Description of the Data Assimilation Systems

A1. TES Assimilation

[38] The TES data are were assimilated in the GEOS-Chem model as described by *Parrington et al.* [2008]. The assimilation approach employed a sequential suboptimal Kalman filer in which the TES ozone profiles were ingested into the model along the TES orbit track with an assimilation cycle of 6 h for 1 July to 31 August 2006. *Parrington et al.* [2008] showed that the assimilation reduced the absolute model bias in the free troposphere from 35% to less than 5% between 300 and 800 hPa, relative to the IONS-6 ozonesonde data across North America. For the results presented here the data were assimilated between 60°S and 60°N using version v7-02-04 of the GEOS-Chem model at a horizontal resolution of 4 × 5. In the assimilation, horizontal correlations in the observation error covariance matrix were neglected, but the TES observations are averaged and assumed uniform across the 4° × 5° gridboxes. The bias in the TES data was accounted for in the assimilation by removing a uniform 3.3 ppb bias in the upper troposphere (for altitudes above 500 hPa) and a 6.5 ppb bias in the lower troposphere as estimated by *Nassar et al.* [2008] for northern midlatitudes in summer. The initial forecast error was assumed to be 50% of the initial ozone distribution and the representativeness error was estimated at 10% on the basis of the sub-grid-scale variability of aircraft data over North America for the INTEX-A and INTEX-B aircraft campaigns. In the TES assimilation the modeled profiles are adjusted only at altitudes below 100 hPa.

[39] The GEOS-Chem CTM [*Bey et al.*, 2001] is a global model driven by assimilated GEOS-4 meteorological fields from GMAO [*Bloom et al.*, 2005]. The native resolution of the GEOS-4 fields is 1° latitude by 1.25° longitude with 55 vertical levels from the surface to 0.01 hPa. As described by *Parrington et al.* [2008], anthropogenic emissions in this version of the model are from the Global Emissions Inventory Activity (GEIA) [*Benkovitz et al.*, 1996], with emissions in the United States based on the Environmental Protection Agency (EPA) National Emission Inventory 1999 (NEI99) [*Hudman et al.*, 2007]. Biomass burning and biofuel emissions are from *Duncan et al.* [2003] and *Yevich and Logan* [2003], respectively. As by *Parrington et al.* [2009], NOx emissions from industrial sources and all anthropogenic emissions of CO have been reduced by 50% and 60%, respectively, relative to the NEI99 values, on the basis of the recommendations of *Hudman et al.* [2007, 2008].

A2. OMI and MLS Assimilation

[40] *Stajner et al.* [2008] assimilated OMI and MLS data into the GMAO GEOS-4 GCM [*Bloom et al.*, 2005]. Ozone was assimilated using a statistical analysis method based on the Physical-Space Statistical Analysis Scheme [*Cohn et al.*, 1998]. MLS ozone profiles were assimilated for pressure levels 0.14 to 215 hPa. In order to exclude OMI data in cloudy regions, only those OMI total ozone columns over locations with reflectivity lower than 15% at 331 nm were assimilated. The assimilation was conducted at the native resolution of the GEOS-4 meteorological fields. For the analysis presented here, the assimilated ozone fields were averaged onto a 4° latitude × 5° longitude grid. Although the assimilation was conducted online in the GEOS-4 GCM, changes in the ozone fields in the assimilation did not influence the radiative transfer calculation in the GCM.

[41] The GEOS-4 GCM does not have an explicit treatment of tropospheric chemistry. Instead, tropospheric ozone chemistry in the assimilation was specified using ozone production (P) and loss (L) rates from version v7–04 of the GEOS-Chem model. These P and L rates were obtained using the same emission inventories imposed in the TES assimilation, but the lightning flash counts in v7–04 of GEOS-Chem were adjusted on the basis of observations from the Optical Transient Detector and the Lightning Imaging Sensor. *Stajner et al.* [2008] showed that the assimilated OMI and MLS fields are in agreement with observations from MOZAIC in the upper troposphere to within 6% in August 2005. Comparison with ozonesondes showed that the mean differences between the assimilated ozone fields and the ozonesonde data in midlatitudes (30°–60°N) between January and June 2005 were less than 10% for pressure levels between 50 and 200 hPa.

[42] **Acknowledgments.** The work described here is performed at the Jet Propulsion Laboratory, California Institute of Technology, under contracts from the National Aeronautics and Space Administration. D. Jones and J. Liu were funded by the Natural Sciences and Engineering Council of Canada and the Canadian Foundation for Climate and Atmospheric Sciences. I. Stajner was supported by NASA's Atmospheric Chemistry Modeling and Analysis Program. We thank Jay Kar for helpful discussions. The views, opinions, and findings contained in this report are those of the author(s) and should not be construed as an official National Oceanic and Atmospheric Administration or U.S. Government position, policy, or decision.

References

Barret, B., et al. (2008), Transport pathways of CO in the African upper troposphere during the monsoon season: A study based upon the assimilation of spaceborne observations, *Atmos. Chem. Phys. Discuss.*, *8*, 2863–2902.

Beer, R., et al. (2001), Tropospheric emission spectrometer for the Earth Observing System's Aura satellite, *Appl. Opt.*, *40*, 2356–2367, doi:10.1364/AO.40.002356.

Benkovitz, C. M., M. T. Scholtz, J. Pacyna, L. Tarrasón, J. Dignon, E. C. Voldner, P. A. Spiro, J. A. Logan, and T. E. Graedel (1996), Global gridded inventories of anthropogenic emissions of sulfur and nitrogen, *J. Geophys. Res.*, *101*(D22), 29,239–29,253, doi:10.1029/96JD00126.

Bey, I., D. J. Jacob, R. M. Yantosca, J. A. Logan, B. D. Field, A. M. Fiore, Q. Li, H. Y. Liu, L. J. Mickley, and M. G. Schultz (2001), Global modeling of tropospheric chemistry with assimilated meteorology: Model description and evaluation, *J. Geophys. Res.*, *106*(D19), 23,073–23,095, doi:10.1029/2001JD000807.

Bloom, S. C., et al. (2005), The Goddard Earth Observing System Data Assimilation System, GEOS DAS version 4.0.3: Documentation and validation, *NASA Tech. Memo., NASA TM-2005–104606*.

Bowman, K. W., et al. (2006), Tropospheric emission spectrometer: Retrieval method and error analysis, *IEEE Trans. Geosci. Remote Sens.*, *44*, 1297–1307, doi:10.1109/TGRS.2006.871234.

Cohn, S. E., A. da Silva, J. Guo, M. Sienkiewicz, and D. Lamich (1998), Assessing the effects of data selection with the DAO Physical–Space Statistical Analysis System, *Mon. Weather Rev.*, *126*, 2913–2926, doi:10.1175/1520-0493(1998)126<2913:ATEODS>2.0.CO;2.

Ding, A., and T. Wang (2006), Influence of stratosphere-to-troposphere exchange on the seasonal cycle of surface ozone at Mount Waliguan in

western China, *Geophys. Res. Lett.*, *33*, L03803, doi:10.1029/2005GL024760.

Duncan, B. N., R. V. Martin, A. C. Staudt, R. Yevich, and J. A. Logan (2003), Interannual and seasonal variability of biomass burning emissions constrained by satellite observations, *J. Geophys. Res.*, *108*(D2), 4100, doi:10.1029/2002JD002378.

Dunkerton, T. J. (1995), Evidence of meridional motion in the summer lower stratosphere adjacent to monsoon regions, *J. Geophys. Res.*, *100*, 16,675–16,688, doi:10.1029/95JD01263.

Fiore, A. M., D. J. Jacob, I. Bey, R. M. Yantosca, B. D. Field, A. C. Fusco, and J. G. Wilkinson (2002), Background ozone over the United States in summer: Origin, trend, and contribution to pollution episodes, *J. Geophys. Res.*, *107*(D15), 4275, doi:10.1029/2001JD000982.

Fu, R., et al. (2006), Short circuit of water vapor and polluted air to the global stratosphere by convective transport over the Tibetan Plateau, *Proc. Natl. Acad. Sci. U. S. A.*, *103*, 5664–5669, doi:10.1073/pnas.0601584103.

Gettelman, A., D. E. Kinnison, T. J. Dunkerton, and G. P. Brasseur (2004), Impact of monsoon circulations on the upper troposphere and lower stratosphere, *J. Geophys. Res.*, *109*, D22101, doi:10.1029/2004JD004878.

Hoskins, B. J., and M. J. Rodwell (1995), A model of the Asian Summer Monsoon. 1. The global-scale, *J. Atmos. Sci.*, *52*, 1329–1340, doi:10.1175/1520-0469(1995)052<1329:AMOTAS>2.0.CO;2.

Hudman, R. C., et al. (2007), Surface and lightning sources of nitrogen oxides over the United States: Magnitudes, chemical evolution and outflow, *J. Geophys. Res.*, *112*, D12S05, doi:10.1029/2006JD007912.

Hudman, R. C., et al. (2008), Biogenic versus anthropogenic sources of CO in the United States, *Geophys. Res. Lett.*, *35*, L04801, doi:10.1029/2007GL032393.

Jiang, J. H., N. J. Livesey, H. Su, L. Neary, J. C. McConnell, and N. A. D. Richards (2007), Connecting surface emissions, convective uplifting, and long-range transport of carbon monoxide in the upper troposphere: New observations from the Aura Microwave Limb Sounder, *Geophys. Res. Lett.*, *34*, L18812, doi:10.1029/2007GL030638.

Jourdain, L., et al. (2007), Tropospheric vertical distribution of tropical Atlantic ozone observed by TES during the northern African biomass burning season, *Geophys. Res. Lett.*, *34*, L04810, doi:10.1029/2006GL028284.

Kar, J., C. R. Trepte, L. W. Thomason, J. M. Zawodny, D. M. Cunnold, and H. J. Wang (2002), On the tropospheric measurements of ozone by the Stratospheric Aerosol and Gas Experiment II (SAGE II, version 6.1) in the tropics, *Geophys. Res. Lett.*, *29*(24), 2208, doi:10.1029/2002GL016241.

Kar, J., et al. (2004), Evidence of vertical transport of carbon monoxide from Measurements of Pollution in the Troposphere (MOPITT), *Geophys. Res. Lett.*, *31*, L23105, doi:10.1029/2004GL021128.

Kulawik, S. S., J. Worden, A. Eldering, K. Bowman, M. Gunson, G. B. Osterman, L. Zhang, S. A. Clough, M. W. Shephard, and R. Beer (2006), Implementation of cloud retrievals for Tropospheric Emission Spectrometer (TES) atmospheric retrievals: 1. Description and characterization of errors on trace gas retrievals, *J. Geophys. Res.*, *111*, D24204, doi:10.1029/2005JD006733.

Kulawik, S. S., et al. (2008), Impact of nonlinearity on changing the a priori of trace gas profiles estimates from the Tropospheric Emission Spectrometer (TES), *Atmos. Chem. Phys. Discuss.*, *8*, 1261–1289.

Kunhikrishnan, T., M. G. Lawrence, R. von Kuhlmann, M. O. Wenig, W. A. H. Asman, A. Richter, and J. P. Burrows (2006), Regional NO_x emission strength for the Indian subcontinent and the impact of emissions from India and neighboring countries on regional O_3 chemistry, *J. Geophys. Res.*, *111*, D15301, doi:10.1029/2005JD006036.

Li, Q., et al. (2001), A tropospheric ozone maximum over the Middle East, *Geophys. Res. Lett.*, *28*(17), 3235–3238.

Liu, J. J., D. B. A. Jones, J. R. Worden, D. Noone, M. Parrington, and J. Kar (2009), Analysis of the summertime buildup of tropospheric ozone abundances over the Middle East and North Africa as observed by the Tropospheric Emission Spectrometer instrument, *J. Geophys. Res.*, *114*, D05304, doi:10.1029/2008JD010993.

Liu, X., et al. (2006), First directly retrieved global distribution of tropospheric column ozone from GOME: Comparison with the GEOS-CHEM model, *J. Geophys. Res.*, *111*, D02308, doi:10.1029/2005JD006564.

Marenco, A., et al. (1998), Measurement of ozone and water vapor by Airbus in-service aircraft: The MOZAIC airborne program, An overview, *J. Geophys. Res.*, *103*(D19), 25,631–25,642.

Moore, G. W. K., and J. L. Semple (2005), A Tibetan Taylor Cap and a halo of stratospheric ozone over the Himalaya, *Geophys. Res. Lett.*, *32*, L21810, doi:10.1029/2005GL024186.

Nassar, R., et al. (2008), Validation of Tropospheric Emission Spectrometer (TES) nadir ozone profiles using ozonesonde measurements, *J. Geophys. Res.*, *113*, D15S17, doi:10.1029/2007JD008819.

Park, M., W. J. Randel, A. Gettelman, S. T. Massie, and J. H. Jiang (2007), Transport above the Asian summer monsoon anticyclone inferred from Aura Microwave Limb Sounder tracers, *J. Geophys. Res.*, *112*, D16309, doi:10.1029/2006JD008294.

Park, M., et al. (2008), Chemical isolation in the Asian monsoon anticyclone observed in Atmospheric Chemistry Experiment (ACE-FTS) data, *Atmos. Chem. Phys.*, *8*, 757–764.

Parrington, M., D. B. A. Jones, K. W. Bowman, L. W. Horowitz, A. M. Thompson, D. W. Tarasick, and J. C. Witte (2008), Estimating the summertime tropospheric ozone distribution over North America through assimilation of observations from the Tropospheric Emission Spectrometer, *J. Geophys. Res.*, *113*, D18307, doi:10.1029/2007JD009341.

Randel, W. J., and M. Park (2006), Deep convective influence on the Asian summer monsoon anticyclone and associated tracer variability observed with Atmospheric Infrared Sounder (AIRS), *J. Geophys. Res.*, *111*, D12314, doi:10.1029/2005JD006490.

Rodgers, C. D. (2000), *Inverse Methods for Atmospheric Sounding: Theory and Practice*, *Ser. Atmos. Oceanic Planet. Phys.*, vol. 2, 238 pp., World Sci., Singapore.

Rodgers, C. D., and B. J. Connor (2003), Intercomparison of remote sounding instruments, *J. Geophys. Res.*, *108*(D3), 4116, doi:10.1029/2002JD002299.

Rodwell, M. J., and B. J. Hoskins (1996), Monsoons and the dynamics of deserts, *Q. J. R. Meteorol. Soc.*, *122*, 1385–1404, doi:10.1002/qj.49712253408.

Rodwell, M. J., and B. J. Hoskins (2001), Subtropical anticyclones and summer monsoons, *J. Clim.*, *14*, 3192–3211, doi:10.1175/1520-0442(2001)014<3192:SAASM>2.0.CO;2.

Sprenger, M., and H. Wernli (2003), A Northern Hemispheric climatology of cross-tropopause exchange for the ERA15 time period (1979–1993), *J. Geophys. Res.*, *108*(D12), 8521, doi:10.1029/2002JD002636.

Stajner, I., et al. (2008), Assimilated ozone from EOS-Aura: Evaluation of the tropopause region and tropospheric columns, *J. Geophys. Res.*, *113*, D16S32, doi:10.1029/2007JD008863.

Thouret, V., A. Marenco, P. Nédélec, and C. Grouhel (1998a), Ozone climatologies at 9–12 km altitude as seen by the MOZAIC Airborne Programme between September 1994 and August 1996, *J. Geophys. Res.*, *103*(D19), 25,653–25,679, doi:10.1029/98JD01807.

Thouret, V., A. Marenco, J. Logan, P. Nédélec, and C. Grouhel (1998b), Comparisons of ozone measurements from the MOZAIC airborne programme and the ozone sounding network at eight locations, *J. Geophys. Res.*, *103*(D19), 25,695–25,720, doi:10.1029/98JD02243.

Worden, H. M., et al. (2007), Comparisons of Tropospheric Emission Spectrometer (TES) ozone profiles to ozonesondes: Methods and initial results, *J. Geophys. Res.*, *112*, D03309, doi:10.1029/2006JD007258.

Worden, H. M., et al. (2008), Satellite measurements of the clear-sky greenhouse effect from tropospheric ozone, *Nature Geosci.*, *1*, 305–308.

Worden, J., S. S. Kulawik, M. W. Shephard, S. A. Clough, H. Worden, K. Bowman, and A. Goldman (2004), Predicted errors of tropospheric emission spectrometer nadir retrievals from spectral window selection, *J. Geophys. Res.*, *109*, D09308, doi:10.1029/2004JD004522.

Worden, J., et al. (2007), Importance of rain evaporation and continental convection in the tropical water cycle, *Nature*, *445*, 528–532, doi:10.1038/nature05508.

Yevich, R., and J. A. Logan (2003), An assessment of biofuel use and burning of agricultural waste in the developing world, *Global Biogeochem. Cycles*, *17*(4), 1095, doi:10.1029/2002GB001952.

R. Beer, K. Bowman, J. Jiang, S. Kulawik, J.-L. F. Li, S. Verma, and J. Worden, Jet Propulsion Laboratory, California Institute of Technology, 4800 Oak Grove Drive, MS 183-301, Pasadena, CA 91109, USA. (john.worden@jpl.nasa.gov)

D. B. A. Jones, J. Liu, and M. Parrington, Department of Physics, University of Toronto, Toronto, ON M5S 1A7, Canada.

I. Stajner, Noblis, Incorporated, 3150 Fairview Park Drive South, Falls Church, VA 22042–4519, USA.

V. Thouret, Laboratoire d'Aérologie, UMR5560, Université de Toulouse, CNRS, 14 Avenue Edouard Belin, F-31400 Toulouse, France.

H. Worden, National Center for Atmospheric Research, P.O. Box 3000, Boulder, CO 80305, USA.